JOURNAL OF AERONAUTICAL MATERIALS
ISSN: 1005-5053

Vol. 43, Issue-01, 2023
pp. 56-82

A CLOSER LOOK AT NEUTRON AND GAMMA SHIELDING BEHAVIORS OF SOME MULTI-CONSTITUENT COMPOSITE MATERIALS

Amit Joshi[a], Kulwinder Singh Mann[b], Genius Walia[a]

[a] Department of Physics, Guru-Kashi University, Talwandi-Sabo, Punjab, India

[b] Department of Physics, D.A.V College, Bathinda-151001, Punjab, India

ABSTRACT

In this study, the shielding properties of four unique lead-free composite materials crafted from industrial waste were examined for their ability to block both neutron and gamma radiation in the energy range of 2-8 MeV. Using specialized tools such as GEANT4, Py-MLBUF, and WinNC, various shielding parameters were analyzed, including the mass attenuation coefficient, buildup factor, kinetic energy released per unit mass, mass effective removal cross-section, half-value layer thickness, and tenth-value layer thickness. The results obtained through GEANT4 and Py-MLBUF were further validated through theoretical calculations using XCOM and Phy-X/PSD, and were found to be within acceptable limits. It was discovered that the multi-constituent composite material made from Brine Sludge had the highest values of mass attenuation coefficient, kinetic energy released per unit mass, and buildup factor at penetration depths of 10 to 40 mfp, making it the most effective material for gamma-ray shielding. Additionally, the advanced tailored radiation shielding material composed of low-Z elements exhibited the highest values of mass effective removal cross-section and the lowest values of half-value and tenth-value layer thickness, making it the best option for neutron shielding. A comprehensive comparison of the radiation shielding abilities of the studied materials and conventional concrete was also provided. These findings suggest that these multi-constituent composite materials may be suitable replacements for concrete in radiation-shielding applications.

Keywords: Nuclear Radiations; Neutron-Gamma Shielding; Lead free materials; Tailored materials from industrial wastage.

1. Introduction

Advanced nuclear technology has a plethora of applications in power generation, medical diagnostics, material and genetic engineering, space exploration, etc. However,

nuclear technology has its own hurdles, like the leakage of ionizing radiations from nuclear establishments and nuclear wastage. The most recent, accidental nuclear radiation leakage at Fukushima, Japan in 2011 emphasized the awful need of improving the safety features by discovering durable and effective shielding materials. The most commonly leaked radiation from nuclear establishments consists of neutrons and gamma rays. Due to deep penetration power, these neutral radiations are difficult to attenuate and therefore cause serious health hazards. Radiation safety standards recommended low-Z materials like high-density polyethene, water, wood, paraffin, etc. for neutron shielding, while on the other hand high-Z materials like oxides of lead, tungsten, uranium, etc. for gamma-ray shielding (Ahmed et al. 2020; Erdem et al. 2010; Rezaei-Ochbelagh and Azimkhani 2012; El-Khayatt 2010). It is to be noted that due to the dominance of Compton-scattering for wide energy range of the gamma rays, investigation of the shielding behavior of a material for mono energetic gamma photons is more complex than that for neutrons. The buildup factor (BUF) parameter measures the contribution of the scattered radiations and plays an important role in study of gamma shielding behaviors (V. P. Singh and Badiger 2012; Amirabadi et al. 2013).

Conventionally, the oxide of Lead (PbO) has been used for nuclear shielding purpose (ANS/ANSI 6.4.3, 1991). Recent confirmation about Lead toxicity demands for its substitute materials. The literature survey indicates that a plethora of publications related to research work on the neutron and gamma-ray shielding efficacies of various materials have been reported as explained in the following section. (Munn and Pontecorvo 1943) investigated and concluded that the combination of water and iron provides good shielding of thermal and resonance neutrons. (Creutz and Downes 1949) had studied the concretes and suggested that magnetite ore concentrate concrete provides better neutron shielding properties than ordinary concrete, possess good tensile strength and ease of handling. (Gugelot and White 1950) reported that concrete mixed with iron and boron has better neutron shielding than ordinary concretes. (Wood 1982) has reported that the boron absorbs thermal neutrons with the emission of charged particles and gamma rays of low energy. Thus, while designing the shielding enclosures for neutrons the gamma-ray shielding must be taken into account.

(El-Hosiny and El-Faramawy 2000) concluded that the portland cement mixed with lead provide better gamma ray shielding than conventional cement. Further, (N. Singh et al. 2004) concluded that bismuth glasses have better gamma ray shielding ability than lead glasses. Moreover, (K. Singh et al. 2015) have compared the gamma-ray shielding abilities of fly ash concretes and concluded that the fly ash concrete with lead offers better shielding and useful in the fly-ash waste management. (Alwaeli 2017) has concluded that the concrete containing

granulated lead-zinc slag waste offers better gamma-ray shielding than conventional concrete. Further, (Olukotun et al. 2019) have investigated the neutron-shielding behavior of various clays and concluded that the clay can be used as neutron shielding material for nuclear facilities. Mann and Joshi (2020) evaluated the radiation shielding capabilities of some engineering materials and concluded that adding small quantities of boron and iron to standard concrete improves its neutron shielding behavior (Kulwinder Singh Mann and Joshi 2020).

Numerous researches have been conducted to develop various radiation-shielding materials, but to our knowledge no progress has been made in the area of lead-free composite materials from industrial waste for neutron and gamma-ray shielding. The present investigation on the neutron and gamma shielding behavior (NGSB) of lead free materials fabricated from the industrial wastage is a novel work. The chosen samples of tailored multi-constituent-composite materials (MCCM) termed as green materials, because these materials has been tailored from the industrial wastage such as Red Mud (RM) and Brine Sludge (BS) (Verma et al. 2017; 2020).

2. Materials and Method

2.1. Materials

The NGSB of have been investigated of some novel lead-free materials chemically tailored from the industrial wastage such as Red Mud (RM) and Brine Sludge (BS). After special chemical treatment of the industrial waste products Advanced Tailored Radiation Shielding Material (ATRSM) has been obtained by Verma *et al*. (Verma et al. 2017; 2021). This material was further blended with the polymeric ester to form thick organo-gel-based materials. The developed shielding gel materials were further cured using glass fiber reinforcement to form radiation shielding panels (SPG) (Verma and Satyabrata 2017). The elemental composition, density, and symbols of all the four samples obtained from literature (Verma and Satyabrata 2017; Verma et al. 2021) have been listed in Table 1.

2.2. Methodology

Investigation of neutron shielding parameters such as mass attenuation coefficient (*MAC*), buildup factor (*BUF*), kinetic energy released per unit mass (*KERMA)*, mass effective removal cross-section (*MERC*), half-value layer thickness (*HVL*), tenth-value layer thickness (*TVL*), etc. have been have been evaluated with standard toolkits viz. GEANT4 (Agostinelli et al. 2003), WinNC Toolkit (K.S. Mann, Heer, and Rani 2015), Py-MLBUF online platform based on standard database of XCOM (NIST) and ANSI/ANS. (K.S Mann and Mann 2021).

2.2.1. GEANT4-Toolkit

The GEANT4 is geometry and tracking computer code that has been developed by CERN in C^{++} (an object-oriented programming language) that simulates the transmission and interaction of various particles with matter, in a broad energy range (eV to GeV). It has wide range of applications in various fields of physics such as high energy physics, medical physics researches, space and nuclear particle physics, etc. (Agostinelli et al. 2003). It allows the individual to derive C++ classes to define geometry, particle generation, and other information classes. G4RunManager is the primary class that must be instantiated, as it manages the entire simulation and controls the programme flow. The primary particle generator, user's detector, and physics list are the other necessary classes. The physics process, geometry, and particle source can be described in these classes. Built-in user commands and G4UserStackingAction are classified to change photon energy, material and kill the secondary particle generated by the primary photon in a run with less computation time. Initially it requires the elemental composition and the mass density of the sample for simulation. Then, after designing the experimental geometry, mono-energetic neutron beam bombarding on a material slab (Fig. 1).

2.2.2 WinNC-Toolkit

The WinNC-Toolkit (K.S. Mann 2015) calculate *MERC* of a material from its chemical composition and mass density using the additive formula and published *MERC* database for fast neutrons (2-12 MeV) (Wood 1982; Kaplan 1989). It has been designed with some extended capabilities, over the similar existing computer programs like ParShield (Elmahroug et al. 2015), MERCSF-N (Elmahroug et al. 2015) and NXcom (El-Khayatt and Akkurt 2013). The missing *MERC* values for elements (Tc, Pm, Po, At, Rn, Fr, Ra, Ac and Pa) in the above mentioned computer programs have been evaluated with bi-quadratic polynomial fitting method with the LINEST function of the MS-Excel (K.S. Mann 2015). Further, WinNC-toolkit has been validated for its computation accuracy of *MERC* using experimental data of some concretes (Rezaei-Ochbelagh and Azimkhani 2012; El-Khayatt 2010; V. P. Singh and Badiger 2012; Amirabadi et al. 2013).The computational methodology of WinNC-toolkit has been described in the flow chart (Fig.2).

2.2.3. Py-MLBUF-Online platform

Py-MLBUF is an acronym of Python-program for Multi-Layered Buildup Factors. Py-MLBUF-online platform is a user friendly and fastest among the similar platforms (BXCOM, and Phy- x/PSD). This open access online platform has been designed has been designed in Python-3 by Mann and Mann (K.S Mann and Mann 2021). For homogeneous and heterogeneous shielding enclosures, the important GSP computed by it are: partial and total

mass attenuation coefficient (*MAC*), exposure buildup factor (*EBF*), energy absorption buildup factor (*EABF*), *HVL*, etc.

3. Results and discussion

The NGSB investigations of the chosen samples have been completed by analyzing of the computed neutron and gamma shielding parameters using the standardized toolkits. Detailed analyses of various parameters have been provided in the following sections:

3.1. Gamma shielding parameters calculations

3.1.1. Mass attenuation coefficient (*MAC*)

The linear attenuation coefficient (*LAC)* describes the fraction of gamma rays that is scattered or absorbed per unit thickness of the shielding material. Mass attenuation coefficient (*MAC*) is another important parameter that measures the probability of all types of interactions of the gamma-photon with shielding material that occurs in the areal thickness of the material. The variation *LAC* and *MAC* of the chosen samples for three gamma energies 2, 6, and 8 MeV have been represented in Fig 3.and Fig.4. The maximum value of *LAC* is for ATRSM but the highest value of *MAC* is for BS in energy range of 2-8 MeV. This is due to the fact that the *LAC* is independent of the density of the material. Density plays a significant role in determining the shielding characteristics of the material. Furthermore, if the *LAC* values divided by the material density we get similar trend (Fig.4). As a result, *MAC* plays a more fundamental role than the *LAC* (K.S. Mann, Rani, and Heer 2015). Py-MLBUF (theoretical method) and GEANT4 code (numerical method) were used to determine the *MAC* for the alloys. The % variation (Fig.5) of the outcomes from both methods is about 0.2 to 1.5 % confirming that numerical and theoretical results are consistent. *MAC* is high at low energy and decreases with increase in energy. For the samples and selected energy range (2-8 MeV), for *MAC*, the descending order of samples is BS (4.36-2.85 mm^2g^{-1}) > RM (4.35-2.6 mm^2g^{-1}) > SPG (4.35-2.58 mm^2g^{-1}) > ATRSM (4.37-2.43 mm^2g^{-1}). At 2 MeV, all the chosen samples have identical the *MAC* values. The reason is that at this intermediate energy range, Compton scattering dominates over other interactions. When the photon energy further exceeds above 4 MeV, the pair production starts dominating for all the samples which is responsible for the increase in mass attenuation coefficient. The variation of mass energy-absorption coefficients (*MenAC*) with energy (Fig.6) of the samples have been found to vary in the following order BS > RM > SPG > ATRSM. The similar trend of mass energy-absorption coefficients (*MenAC)* supports the above conclusion. The

comparison of gamma shielding characteristics of MCCM samples with various concrete (Bashter 2006; 1997) is represented in Fig 5. It can be seen that ordinary concrete have high gamma shielding ability than the selected MCCM samples. But *MAC* value of BS is greater than other two reference concrete (SMC and BMC). This indicates that BS is highly capable for gamma shielding.

3.1.2. *KERMA* relative to the air

The variation of *KERMA* relative to the air (K_R) with the photon energy of the samples is shown in Fig. 7. The highest value of K_R was for BS, which indicates that the kinetic energy released per unit mass in BS was high (V. P. Singh, Badiger, and El-Khayatt 2014). Therefore, Gamma-ray energy loss in BS was high. This is because BS contains a high Z element such as Ba (24.57%), Ca (14.38%) to remove gamma photons. The K_R of the samples have been observed in the following order BS > RM > SPG > ATRSM. It was found that BS provides better gamma shielding due to higher removal capacity in selected energy range.

3.1.3. Buildup factor (*BUF*)

The variation of *BUF* with incident photon energy for each samples studied at fixed penetration depth of 0.5, 5, 10, 20, 30 and 40 mfp has been shown in Fig.8. *BUF* values peak at energy 2 MeV, and then start decreasing. In this energy range, Compton scattering is a dominant photon interaction process that only contributes to the degradation of the photon energy due to scattering and does not remove the photon completely. The lifetime of the photon is longer and therefore, the photon is more likely to escape from the sample. This process leads to an increase in the *BUF* value. In the low-energy regime, the photoelectric effect is the dominant photon interaction process, the cross-section of which changes with energy as $1/E^3$. Due to the dominance of this process, the maximum numbers of the photons are absorbed. Similarly, in the higher energy region, pair production is the dominant one, whose cross-section varies inversely with energy as E^2 (V. P. Singh and Badiger 2014; H. Singh et al. 2016). Due to multiple scattering events at large penetration depths, the values of *BUF* became very high for the penetration depth of 40 mfp.The *BUF* values at photon energy 2 MeV were found to be 1.34–57.24, 1.36 –60.03, 1.35–60.51, and 1.36–60.01 for BS, RM, ATRSM, and SPG, respectively for penetration depths of 1-40 mfp. In the high energy regions (>2 MeV), *BUF* values were increasing for 20 and 40 mfp penetration depth. The *BUF* values for BS reached a maximum of up to 84.62 at the penetration depth of 40 mfp. The chemical composition of MCCM caused this variation (Mann and Korkut 2013; Al-Buriahi and Mann 2019). Fig.9 shows that *Zeq* is the lowest in ATRSM and the highest in BS. This is due to the presence of low-Z elements such as C (46.8%) and O (26.8%) in ATRSM. The pair-production is directly

proportional to Z^2, so the low value of *Zeq* exhibits the lowest value of *BUF* at high energy (>2 MeV). The gamma ray shielding characteristics of the material directly depends on the *Zeq* value i.e. material with higher *Zeq* values have high ability to attenuate gamma rays (Mann, Rani, and Heer 2015). So BS appear to be most effective and ATRSM appear to least effective material for gamma ray shielding

The variation of B*UF* has been studied with penetration depth at fixed energies are shown in Fig. 10. In general, it has been observed that *BUF* varies directly with penetration depth. At incident photon energy of 2 MeV (Fig. 10(a)) the *BUF* values for different samples are almost the same. The *BUF* value of MCCM is between 1.3374 and 11.2868 for penetration depths of 1-10 mfp. At high incident photon energies of 6-8 MeV (Fig. 10 (b-c)) and penetration depths greater than 10 mfp, BS exhibits maximum *BUF* values, whereas ATRSM exhibits minimum *BUF* values. This trend can be explained on the basis that, at this incident photon energy (i.e., 6–8 MeV), pair production is the dominant photon interaction process.

3.2. Neutron interaction parameters

The *MERC* is an important parameter that describe material's neutron shielding ability. Higher the value of *MERC* of materials indicates its better efficacy in attenuating the traversing neutron beam (El-Khayatt 2010; Tellili, Elmahroug, and Souga 2014). The neutron shielding parameter *MERC* for the MCCM samples was evaluated by using WinNC-Toolkit and GEANT4 code. The comparisons of the outcomes are shown in Fig. 12. The results have been observed similar trend. The values of *MERC* calculated with GEANT4 code for the MCCM in the selected energy range were in ascending order of BS < RM < SPG < ATRSM. The *MERC* values decreases with increase in energy (Fig. 13).The values of the *MERC* ranges from 4.6215 to 3.3209, 4.778 to 3.626, 4.943 to 4.124 and 6.606 to 4.6343 mm^2g^{-1} for BS, RM, SPG and ATRSM respectively in the selected energy range. Since *MERC* is density-dependent, it increases with density (Bashter, Makarious, and Abdo 1996). Maximum value of *MERC* was observed for ATRSM due to its high density and its composition of low-Z element, C (46.8%) and O (26.8%); which plays an important role in slowing down and capture of neutrons. To assess the neutron shielding capability of MCCM, it is vital to compare them with various concrete reported previously. For this purpose, the *MERC* of the MCCM used in this study was compared with three different samples of concrete (Bashter 2006; 1997). All the selected MCCM samples have higher *MERC* than OC, SMC, and BMC (Fig. 16). Thus, the selected MCCM studied in this investigation have better neutron attenuation ability than the concretes. *HVL* and *TVL* indicate how deeply radiation of certain energy could penetrate a material. The variations of these parameters with density and energy for the chosen samples have been

demonstrated in Figs. 14 and 15. The *HVL* and *TVL* values of prepared samples have been found to vary in the following order ATRSM < SPG < BS < RM, while the density of the samples have been observed in the decreasing order of ATRSM > SPG > BS > RM. However, the *HVL* and *TVL* values were small at 2 MeV but, increases with increase in energy for all MCCM samples. The dependence of these parameters on density and chemical composition can be clearly observed such that, the ATRSM with high-density and comprising low-Z elements has the lowest value and BS with low-density and comprising high-Z elements has the highest values *HVL* and *TVL*. Lower the values of *HVL* and *TVL*, the greater the shielding efficacy of the material (Sadawy and El Shazly 2019; Aygün 2019). It has been concluded that the ATRSM (high density) offers the highest shielding for neutrons.

4.Conclusions

In conclusion, our investigations of various neutron and gamma-ray shielding parameters, as well as the neutron and gamma shielding behaviors (NGSB) of the multi-constituent composite materials (MCCM), have yielded some noteworthy findings. Firstly, it has been determined that the mass attenuation coefficients (*MAC*) of multi-constituent composite materials (MCCM) are comparable to those of various types of concrete. Additionally, it was observed that the mass attenuation coefficient (*MAC*) of Brine Sludge (BS) is the highest among the selected multi-constituent composite materials, and thus confirms that BS offers the utmost gamma-ray shielding in the energy range of 2-8 MeV among the selected samples. Furthermore, Brine Sludge (BS) was found to have the highest *BUF* in the energy range of 6 to 8 MeV at 10-40 mfp penetration depths. Furthermore, it was found that *KERMA* relative to air of Brine Sludge is greater than that of other investigated materials.

In addition to this, we discovered that high-density materials comprising low-Z elements exhibit high mass effective removal cross-section. The highest and lowest mass effective removal cross-section (*MERC*) values were observed for ATRSM and BS, respectively. ATRSM have higher mass effective removal cross-section (*MERC*) than concrete. Thus, the advance tailored radiation shielding material (ATRSM) offers the utmost neutron shielding in the energy range of 2-8 MeV. Additionally, it was found that the half-value layer (*HVL*) and Tenth-value layer (*TVL*) of advance tailored radiation shielding material (ATRSM) is the lowest among the selected multi-constituent composite materials, confirming that ATRSM are effective for attenuating fast neutrons in the selected energy range.

Finally, it was determined that double-layered enclosures made from the combination of both ATRSM and BS provides good neutron and gamma shielding behavior (NGSB) in the

chosen energy range of 2-8 MeV. It is clear that the MCCM tailored from industrial wastage have the potential to produce cost-effective and Lead-free substitutes for the conventional radiation shielding materials. Furthermore, the tailored radiation shielding materials may aid in industrial waste management. Therefore, in the future, more research is required in this direction to explore the hidden potential of industrial waste.

Acknowledgements:

With profound gratitude, we acknowledge the invaluable assistance rendered to us by the GEANT4-toolkit, WinNC toolkit, and Py-MLBUF-platform in the course of our research. Their open-access facilities proved to be a crucial aspect of our investigation. We must also express our sincere appreciation for the fact that we received no funding for this endeavor.

References:

Agostinelli, S., J. Allison, K. Amako, J. Apostolakis, H. Araujo, P. Arce, M. Asai, et al. 2003. "GEANT4 - A Simulation Toolkit." *Nuclear Instruments and Methods in Physics Research, Section A: Accelerators, Spectrometers, Detectors and Associated Equipment* 506 (3): 250–303. https://doi.org/10.1016/S0168-9002(03)01368-8.

Ahmed, Bashir, G. B. Shah, Azhar H. Malik, Aurangzeb, and M. Rizwan. 2020. "Gamma-Ray Shielding Characteristics of Flexible Silicone Tungsten Composites." *Applied Radiation and Isotopes* 155 (June 2019): 108901. https://doi.org/10.1016/j.apradiso.2019.108901.

Alwaeli, Mohamed. 2017. "Investigation of Gamma Radiation Shielding and Compressive Strength Properties of Concrete Containing Scale and Granulated Lead-Zinc Slag Wastes." *Journal of Cleaner Production* 166: 157–62. https://doi.org/10.1016/j.jclepro.2017.07.203.

Amirabadi, Eskandar Asadi, Marzieh Salimi, Nima Ghaleh, Gholamreza Etaati, and and Hossien Asadi. 2013. "Study of Neutron and Gamma Radiation Protective Shield." *International Journal of Innovation and Applied Studies* 3 (4): 1079–85. http://www.issr-journals.org/ijias/abstract.php?article=IJIAS-13-156-06.

Aygün, Bünyamin. 2019. "High Alloyed New Stainless Steel Shielding Material for Gamma and Fast Neutron Radiation." *Nuclear Engineering and Technology*, no. xxxx. https://doi.org/10.1016/j.net.2019.08.017.

Bashter, I. 1997. "Calculation of Radiation Attenuation Coefficients for Shielding Concretes." *Annals of Nuclear Energy* 24 (17): 1389–1401. https://doi.org/10.1016/S0306-4549(97)00003-0.

Bashter, I. 2006. "Radiation Attenuation and Nuclear Properties of High Density Concrete Made with Steel Aggregates." *Radiation Effects and Defects in Solids* 140: 37–41. https://doi.org/10.1080/10420159708216859.

Bashter, I.I, A.S. Makarious, and A.EL-Sayed Abdo. 1996. "Investigation of Hematite - Serpentine and Ilmenite- Limonite Concretes for Reactor Radiation Shielding." *Ann. Nucl. Energy* 23 (1): 65–71.

Creutz, E., and K. Downes. 1949. "Magnetite Concrete for Radiation Shielding." *Journal of Applied Physics* 20 (12): 1236–40. https://doi.org/10.1063/1.1698315.

El-Hosiny, F. I., and N. A. El-Faramawy. 2000. "Shielding of Gamma Radiation by Hydrated Portland Cement-Lead Pastes." *Radiation Measurements* 32 (2): 93–99. https://doi.org/10.1016/S1350-4487(99)00050-5.

El-Khayatt, A. M. 2010. "Calculation of Fast Neutron Removal Cross-Sections for Some Compounds and Materials." *Annals of Nuclear Energy* 37 (2): 218–22. https://doi.org/10.1016/j.anucene.2009.10.022.

El-Khayatt, A. M., and I. Akkurt. 2013. "Photon Interaction, Energy Absorption and Neutron Removal Cross Section of Concrete Including Marble." *Annals of Nuclear Energy* 60: 8–14. https://doi.org/10.1016/j.anucene.2013.04.021.

Elmahroug, Y., B. Tellili, C. Souga, and K. Manai. 2015. "ParShield: A Computer Program for Calculating Attenuation Parameters of the Gamma Rays and the Fast Neutrons." *Annals of Nuclear Energy* 76: 94–99. https://doi.org/10.1016/j.anucene.2014.09.044.

Erdem, Mehmet, Oktay Baykara, Mahmut Doğru, and Fatih Kuluöztürk. 2010. "A Novel Shielding Material Prepared from Solid Waste Containing Lead for Gamma Ray." *Radiation Physics and Chemistry* 79 (9): 917–22. https://doi.org/10.1016/j.radphyschem.2010.04.009.

Gugelot, P C, and M G White. 1950. "On the Shielding Qualities of Different Concrete Mixtures" 369. https://doi.org/10.1063/1.1699669.

Kaplan, M F. 1989. *Concrete Radiation Shielding*. New York, NY (USA): John Wiley and Sons Inc.

Mann, K.S. 2015. "Toolkit for Fast Neutron Removal Cross-Section." In *3rd International Conference Advancements in Engineering and Technology*. Sangrur (Puanjab), India.: Bhai Gurdas Institute of Engineering and Technology.

Mann, K.S., M.S. Heer, and A. Rani. 2015. "Fast Neutron Removal Cross-Section Calculations: Computer Program." *International Journal of Application or Innovation in Engineering & Management*, 1–17. https://www.ijaiem.org/pabstract2.php?pid=IJAIEM-2015-02-08-14.

Mann, K.S., Asha Rani, and Manmohan Singh Heer. 2015. "Shielding Behaviors of Some Polymer and Plastic Materials for Gamma-Rays." *Radiation Physics and Chemistry* 106: 247–54. https://doi.org/10.1016/j.radphyschem.2014.08.005.

Mann, K.S, and S.S Mann. 2021. "Py-MLBUF: Development of an Online-Platform for Gamma-Ray Shielding Calculations and Investigations." *Annals of Nuclear Energy* 150: 107845. https://doi.org/10.1016/j.anucene.2020.107845.

Mann, Kulwinder Singh, and Amit Joshi. 2020. *Advances in Wireless Communication and*

Mathematics. Edited by Ram Krishan and Lekh Raj. First. Patiala: Twenty first century publications.

Manohara, S. R., S. M. Hanagodimath, and L. Gerward. 2008. "Studies on Effective Atomic Number, Electron Density and Kerma for Some Fatty Acids and Carbohydrates." *Physics in Medicine and Biology* 53 (20): 377–86. https://doi.org/10.1088/0031-9155/53/20/N01.

Munn, A.M, and B. Pontecorvo. 1943. "Spatial Distribution of Neutrons in Hydrogenous Media Containing Bismuth,Lead and Iron." *Canadian Journal of Research* 25: 157–67.

Olukotun, S. F., Kulwinder Singh Mann, S. T. Gbenu, F. I. Ibitoye, O. F. Oladejo, Amit Joshi, H. O. Tekin, et al. 2019. "Neutron-Shielding Behaviour Investigations of Some Clay-Materials." *Nuclear Engineering and Technology* 51 (5): 1444–50. https://doi.org/10.1016/j.net.2019.03.019.

Rezaei-Ochbelagh, D., and S. Azimkhani. 2012. "Investigation of Gamma-Ray Shielding Properties of Concrete Containing Different Percentages of Lead." *Applied Radiation and Isotopes* 70 (10): 2282–86. https://doi.org/10.1016/j.apradiso.2012.06.020.

Rinard, P. 1990. "Neutron Interactions with Matter." *Los Alamos Technical Reports*, 357–77.

Sadawy, M. M., and R. M. El Shazly. 2019. "Nuclear Radiation Shielding Effectiveness and Corrosion Behavior of Some Steel Alloys for Nuclear Reactor Systems." *Defence Technology* 15 (4): 621–28. https://doi.org/10.1016/j.dt.2019.04.001.

Singh, Kanwaldeep, Sukhpal Singh, A. S. Dhaliwal, and Gurmel Singh. 2015. "Gamma Radiation Shielding Analysis of Lead-Flyash Concretes." *Applied Radiation and Isotopes* 95: 174–79. https://doi.org/10.1016/j.apradiso.2014.10.022.

Singh, Narveer, Kanwar Jit Singh, Kulwant Singh, and Harvinder Singh. 2004. "Comparative Study of Lead Borate and Bismuth Lead Borate Glass Systems as Gamma-Radiation Shielding Materials." *Nuclear Instruments and Methods in Physics Research, Section B: Beam Interactions with Materials and Atoms* 225 (3): 305–9. https://doi.org/10.1016/j.nimb.2004.05.016.

Singh, Vishwanath P., and N. M. Badiger. 2012. "Comprehensive Study of Energy Absorption and Exposure Build-up Factors for Concrete Shielding in Photon Energy Range 0.015-15 MeV up to 40 Mfp Penetration Depth: Dependency of Density, Chemical Elements, Photon Energy." *International Journal of Nuclear Energy Science and Technology* 7 (1): 75–99. https://doi.org/10.1504/IJNEST.2012.046987.

Singh, Vishwanath P., N. M. Badiger, and A. M. El-Khayatt. 2014. "Study on γ-Ray Exposure Buildup Factors and Fast Neutron-Shielding Properties of Some Building Materials." *Radiation Effects and Defects in Solids* 169 (6): 547–59. https://doi.org/10.1080/10420150.2014.905942.

Tellili, B., Y. Elmahroug, and C. Souga. 2014. "Calculation of Fast Neutron Removal Cross Sections for Different Lunar Soils." *Advances in Space Research* 53 (2): 348–52. https://doi.org/10.1016/j.asr.2013.10.023.

Verma, Sarika, S. S. Amritphale, Sunil Kumar Sanghi, and Satyabrata Das. 2017.

"Development of Functional Material for Simultaneous Shielding X-Ray and EMI Radiations Using Inorganic–Organic Hybrid Gel." *Journal of Inorganic and Organometallic Polymers and Materials* 27 (3): 728–38. https://doi.org/10.1007/s10904-017-0517-9.

Verma, Sarika, Medha Mili, Harsh Bajpai, S. A.R. Hashmi, and A. K. Srivastava. 2021. "Advanced Lead Free, Multi-Constituent-Based Composite Materials for Shielding against Diagnostic X-Rays." *Plastics, Rubber and Composites* 50 (2): 48–60. https://doi.org/10.1080/14658011.2020.1831264.

Verma, Sarika, Medha Mili, Harsh Bajpai, S A R Hashmi, and A K Srivastava. 2020. "Plastics , Rubber and Composites Advanced Lead Free , Multi-Constituent-Based Composite Materials for Shielding against Diagnostic X-Rays." *Plastics, Rubber and Composites*, 1–13. https://doi.org/10.1080/14658011.2020.1831264.

Verma, Sarika, and S S Amritphale Satyabrata. 2017. "Development of Advanced , X-Ray Radiation Shielding Panels by Utilizing Red Mud-Based Polymeric Organo-Shielding Gel-Type Material." *Waste and Biomass Valorization* 8 (6): 2165–75. https://doi.org/10.1007/s12649-016-9701-3.

Wood, James. 1982. *Computational Methods in Reactor Shielding*. First. Oxford: Pergamon Press.

Table captions

Table 1. Elemental composition of the multi-constituent-based composite materials

List of Figures

Figure 1. Simulation Geometry used in the GEANT4 toolkit

Figure 2. Flow Chart of WinNC-Toolkit (K.S. Mann, Heer, and Rani 2015)

Figure 3. The variation of *LAC* of the samples with energy

Figure 4. The variation of *MAC* of the samples with energy

Figure 5. Comparison of GEANT4 and Py-MLBUF online platform for calculation of *MAC*

at three gamma-ray energies viz. 2, 6, and 8 MeV.

Figure 6. The variation of *MenAC* of the samples with energy

Figure 7. Variation of *KERMA* with energy of the samples

Figure 8. Comparative variation of *BUF* for the samples with energies 2, 6, and 8 MeV at various penetration depths: 0.5, 10, 15, 20, 30 and 40 mfp.

Figure 9. Relative variation of *Zeq* of the samples with energy

Figure 10. Variation of *BUF* at different penetration depth of the samples with energy

Figure 11. Comparison of *MAC* values of MCCM samples with various concrete

Figure 12. Comparison of GEANT4 and WinNC-Toolkit for calculation of *MERC* at three neutron energies viz. 2, 6, and 8 MeV.

Figure 13. Variations of *MERC* with density of the samples at energies 2, 6, and 8 MeV

Figure 14. Variations of *HVL* with density of the samples at energies 2, 6, and 8 MeV

Figure 15. Variations of *TVL* with density of the samples at energies 2, 6, and 8 MeV

Figure 16. Comparison of *MERC* values of MCCM samples with various concrete at three energies viz. 2, 6, and 8 MeV**.**

Table 1: Elemental composition of the multi-constituent-based composite materials (MCCM)

S. No.	Sample (MCCM)	Symbol	Density ($g\ cm^{-3}$)	Chemical Composition (Verma and Satyabrata 2017; Verma et al. 2021)
1	Radiation shielding panel	SPG	3.09	0.0399Al+0.0947C+0.344O+0.0239Si+0.0063P+0.0085Ca +0.149Ti+0.318Fe+0.0104Na
2	Advance Tailored Radiation Shielding Material	ATRSM	3.90	0.0201Al+0.468C+0.268O+0.0184Si+0.0165Ca+0.0156Ti+0.0609Fe +0.0081Na+0.0137Mg+0.0099Cl+0.0822Ba+0.0182S
4	Red Mud	RM	2.10	0.3813O+0.1081Al+0.0511Si+0.0045P+0.0021K+0.0197Ca+0.1087Ti +0.0027V+0.3183Fe+0.0017Zr
5	Brine Sludge	BS	2.52	0.0793Mg+0.0181Al+0.0524Si+0.0031P+0.0490S+0.0634Cl+0.0039K +0.1438Ca+0.0254Fe+0.2457Ba+0.0062Sr+0.303974O

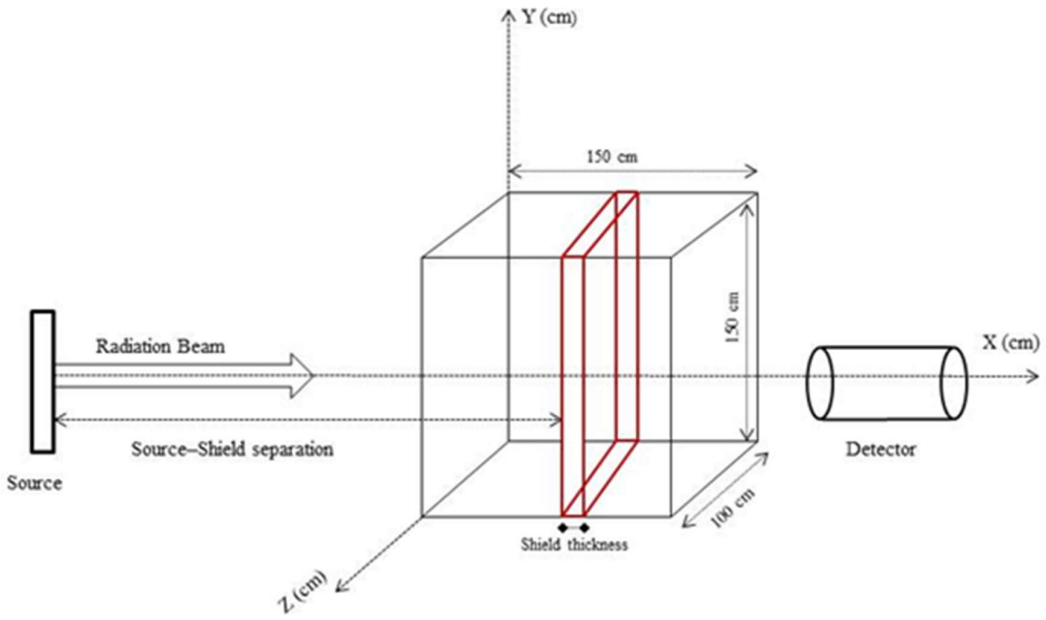
Y (cm)
150 cm
150 cm
Radiation Beam
X (cm)
Source–Shield separation
Source
Detector
100 cm
Shield thickness
Z (cm)

Fig 1.

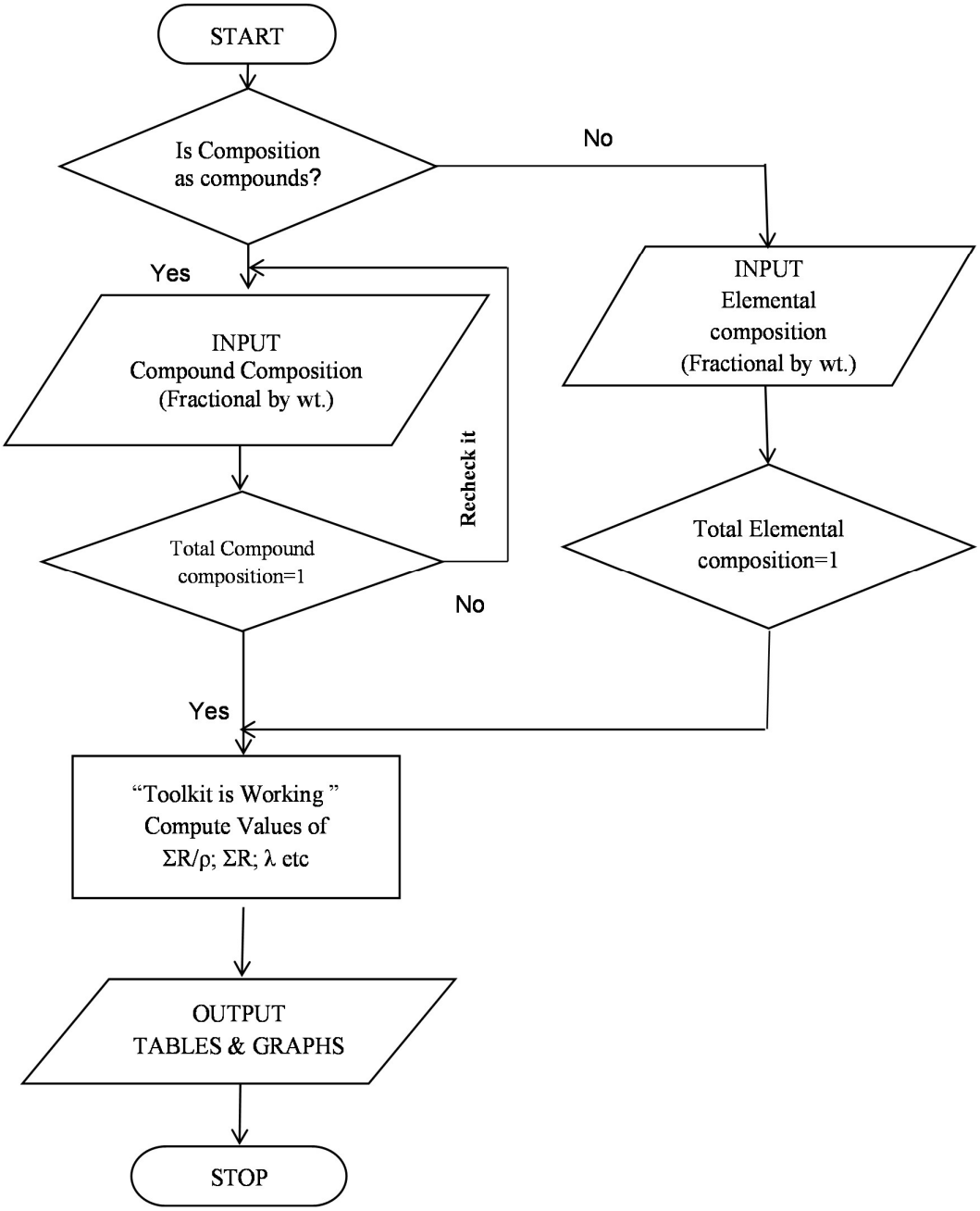
START
Is Composition as compounds?
No
Yes
INPUT Compound Composition (Fractional by wt.)
Recheck it
Total Compound composition=1
No
INPUT Elemental composition (Fractional by wt.)
Total Elemental composition=1
Yes
"Toolkit is Working " Compute Values of ΣR/ρ; ΣR; λ etc
OUTPUT TABLES & GRAPHS
STOP

Fig. 2.

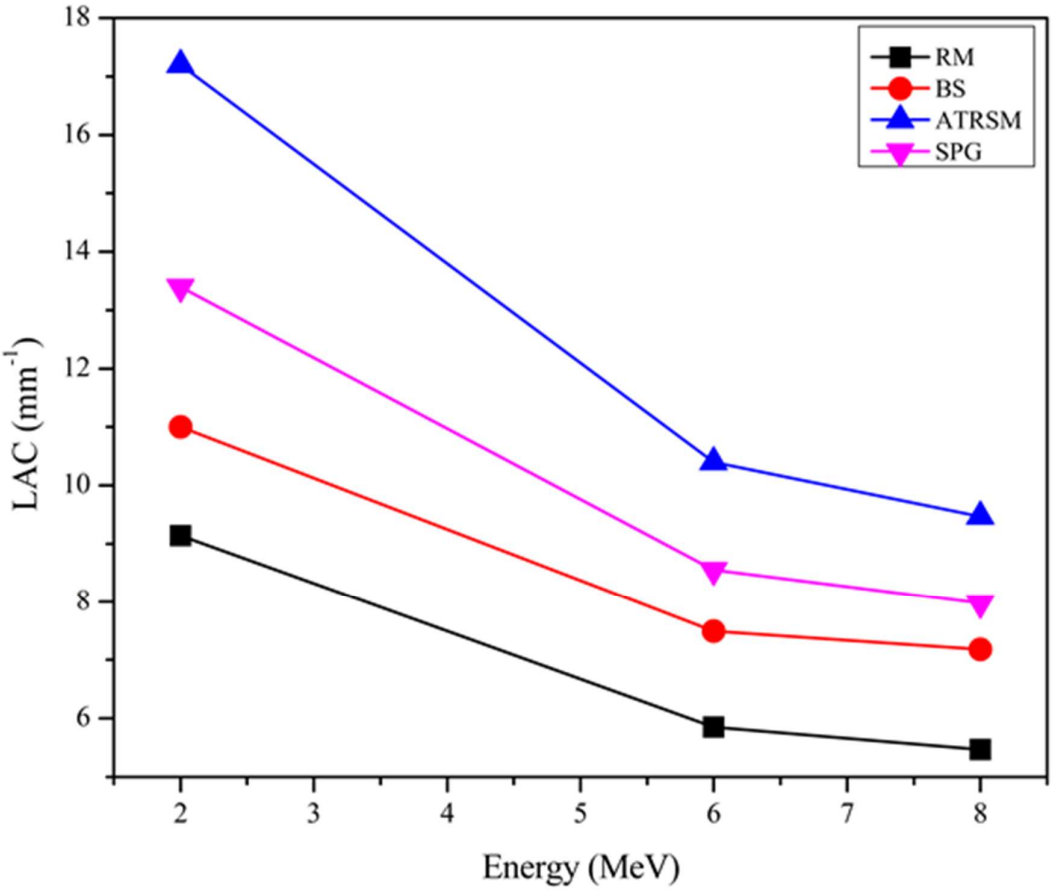

Fig. 3.

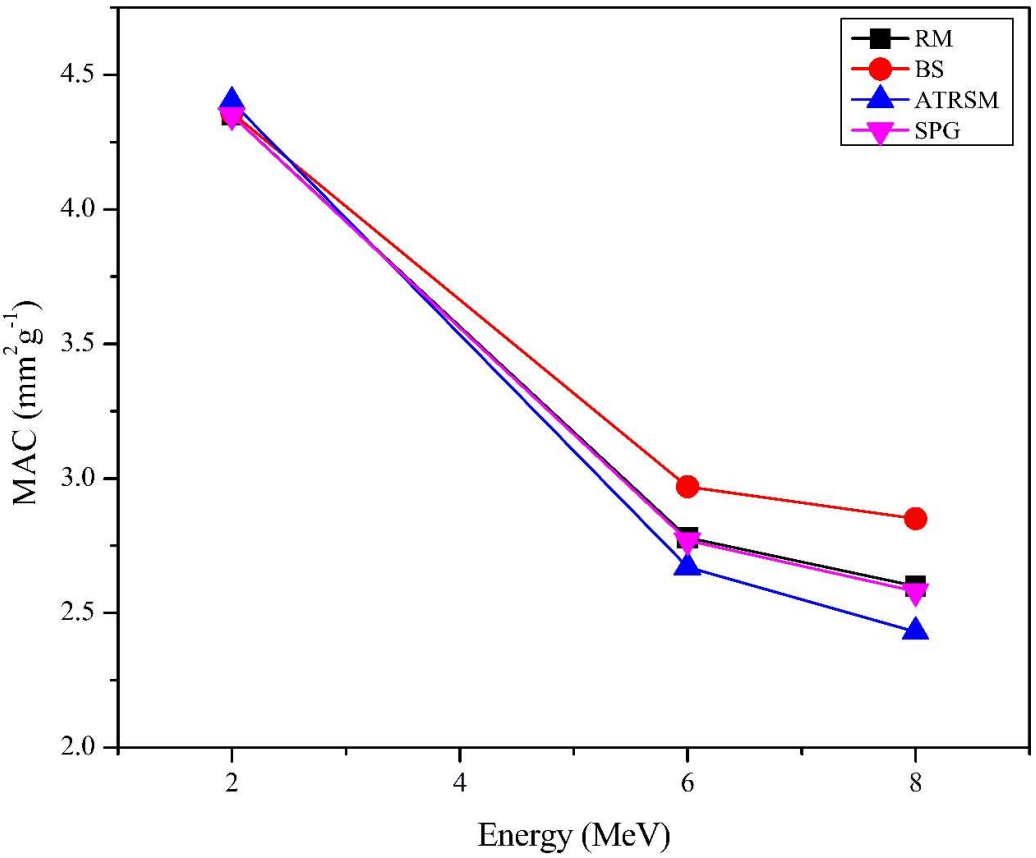

Fig. 4.

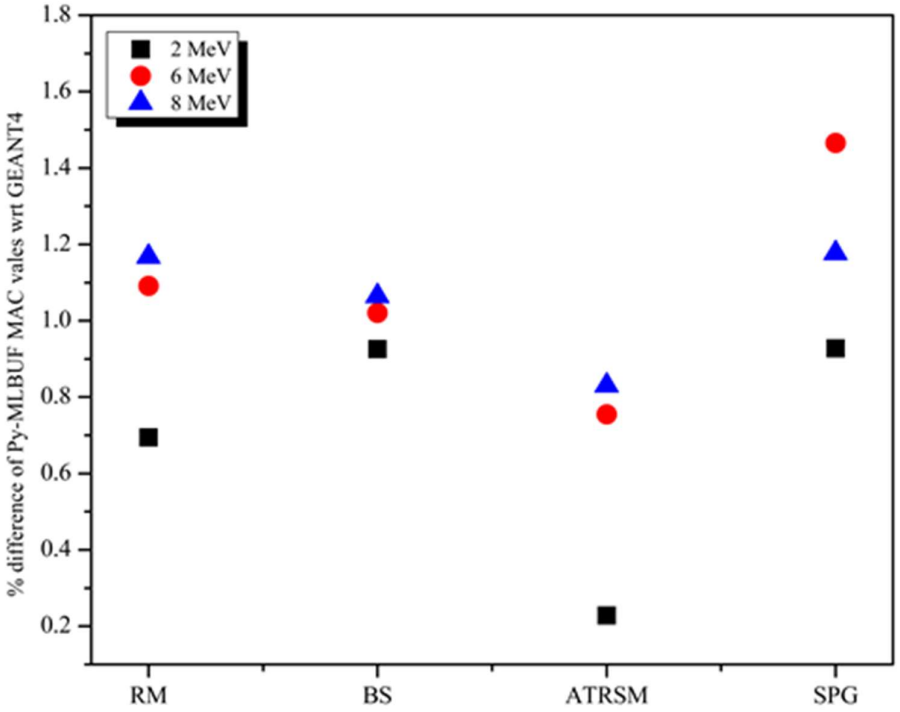
2 MeV
6 MeV
8 MeV
% difference of Py-MLBUF MAC vales wrt GEANT4
1.8
1.6
1.4
1.2
1.0
0.8
0.6
0.4
0.2
RM
BS
ATRSM
SPG

Fig.5.

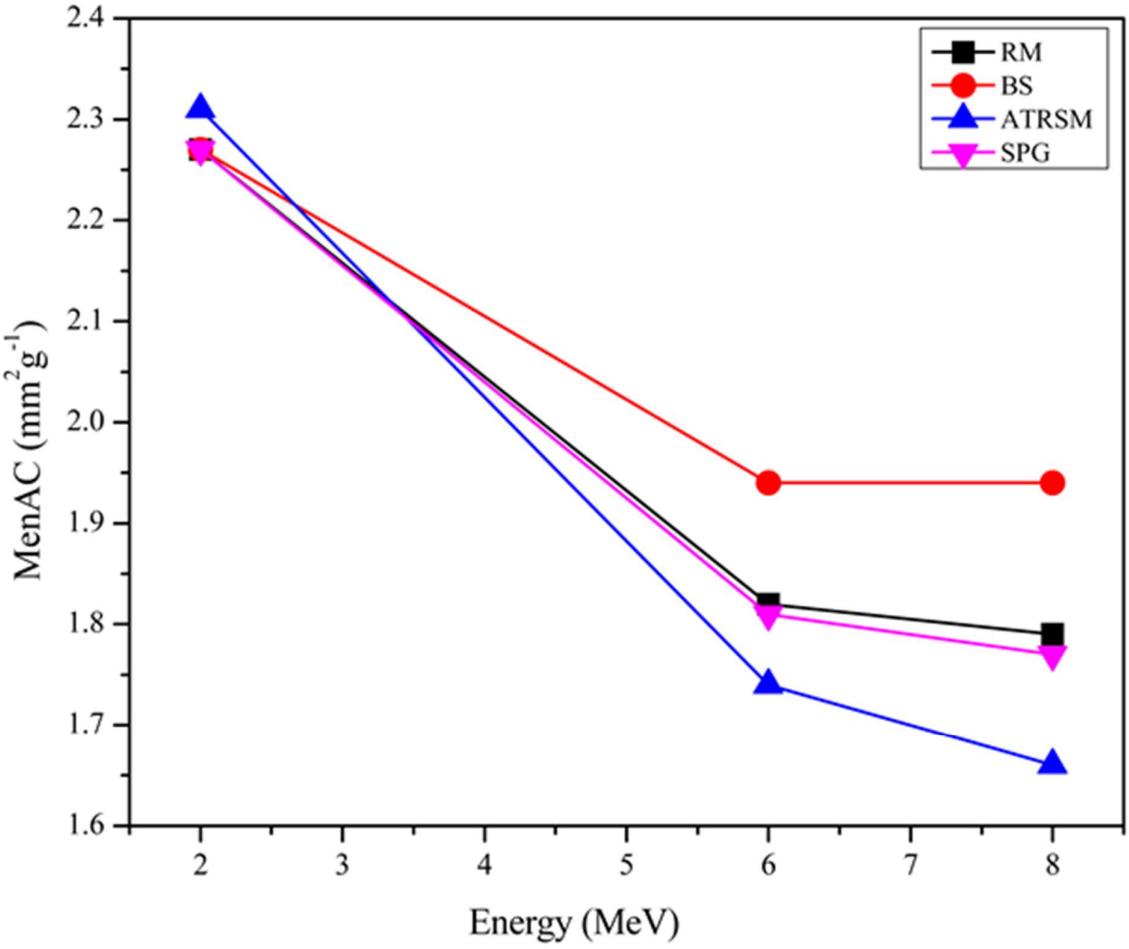
RM
BS
ATRSM
SPG
MenAC (mm^{2}g^{-1})
Energy (MeV)
2.4
2.3
2.2
2.1
2.0
1.9
1.8
1.7
1.6
2
3
4
5
6
7
8

Fig. 6.

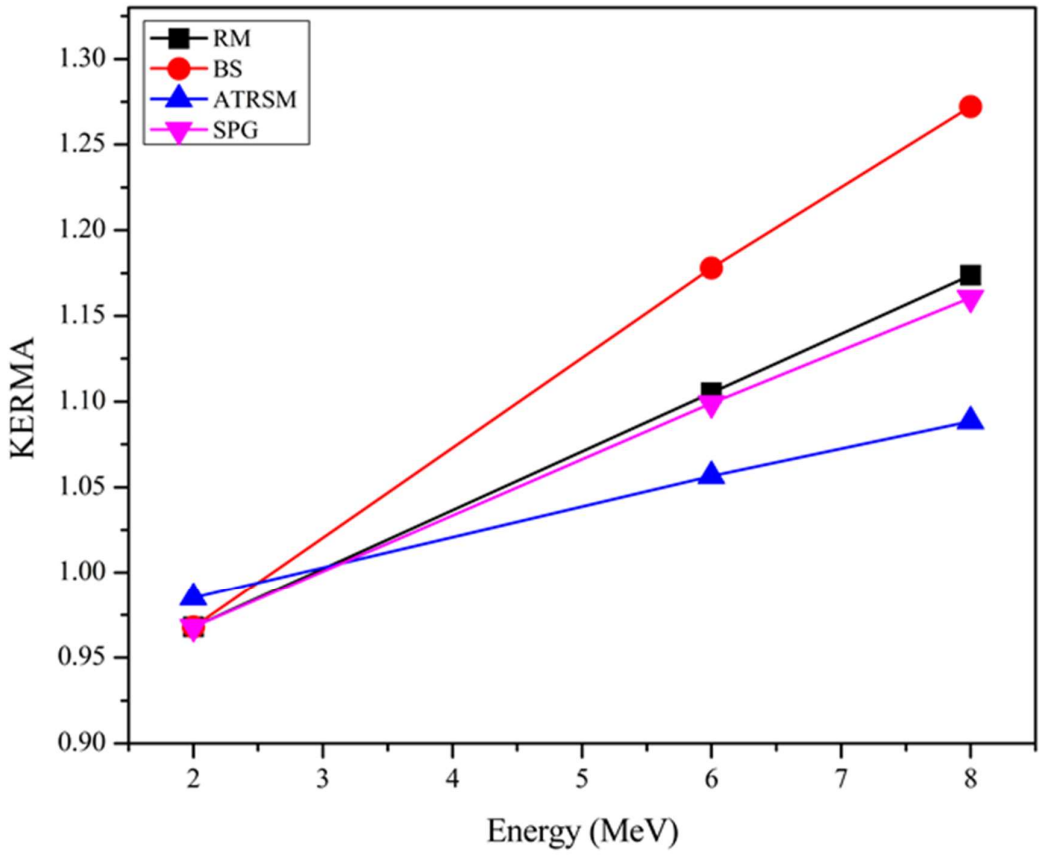
RM
BS
ATRSM
SPG
KERMA
1.30
1.25
1.20
1.15
1.10
1.05
1.00
0.95
0.90
2
3
4
5
6
7
8
Energy (MeV)

Fig. 7.

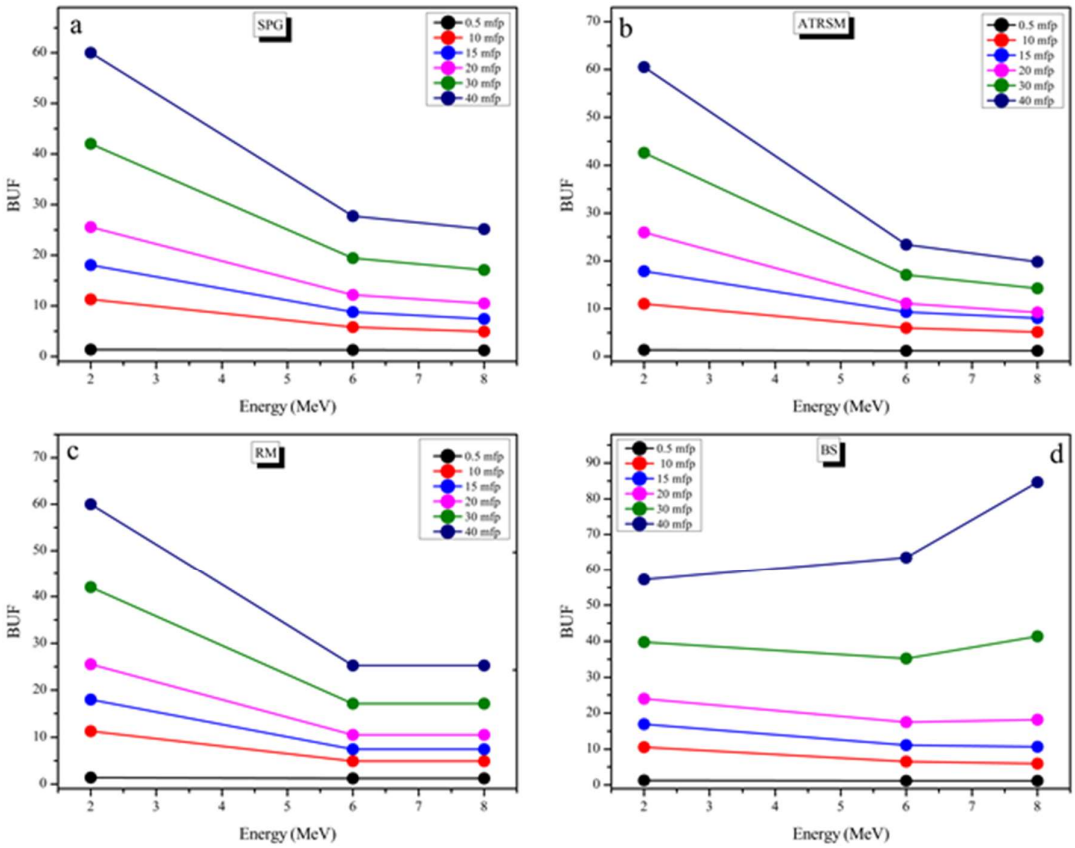
a
SPG
b
ATRSM
c
RM
d
BS
0.5 mfp
10 mfp
15 mfp
20 mfp
30 mfp
40 mfp
BUF
Energy (MeV)

Fig.8.

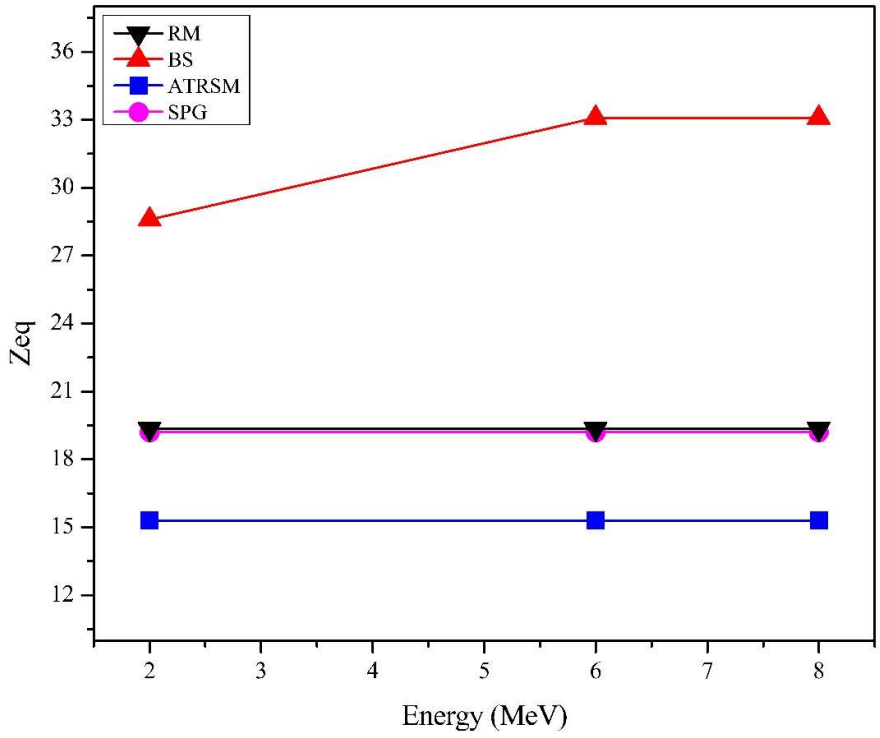

Fig.9.

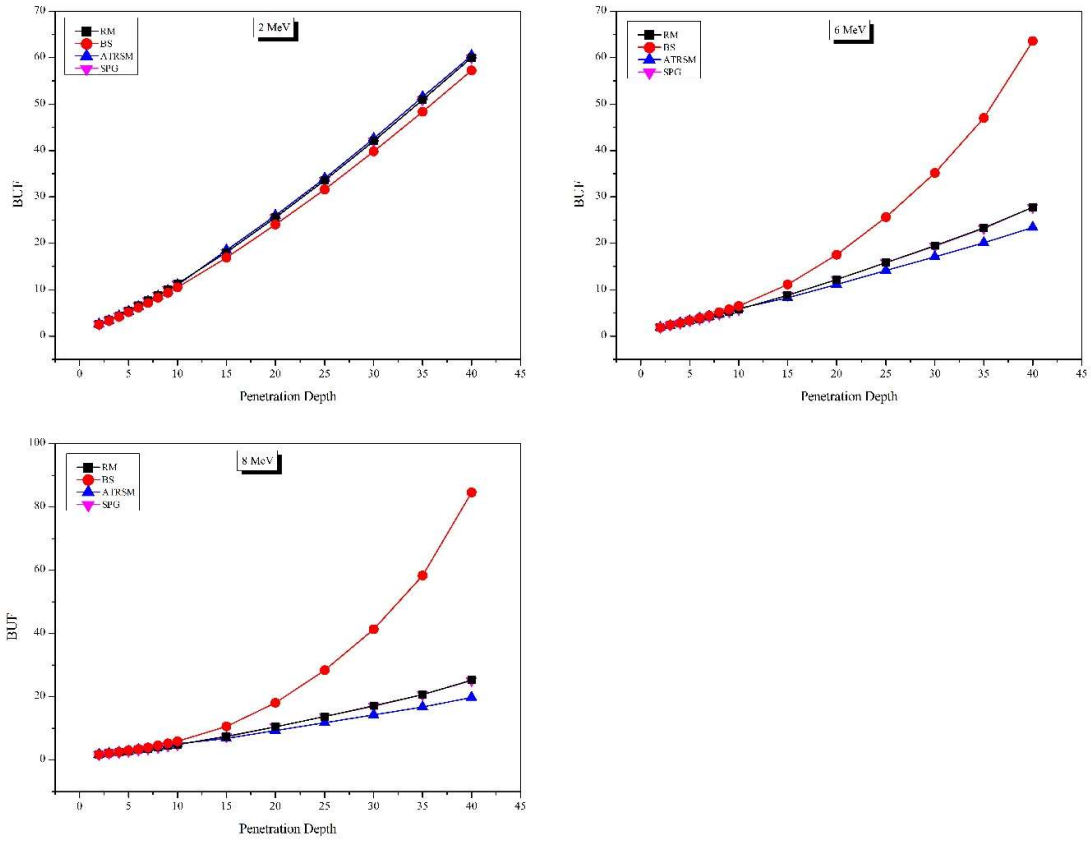

Fig. 10.

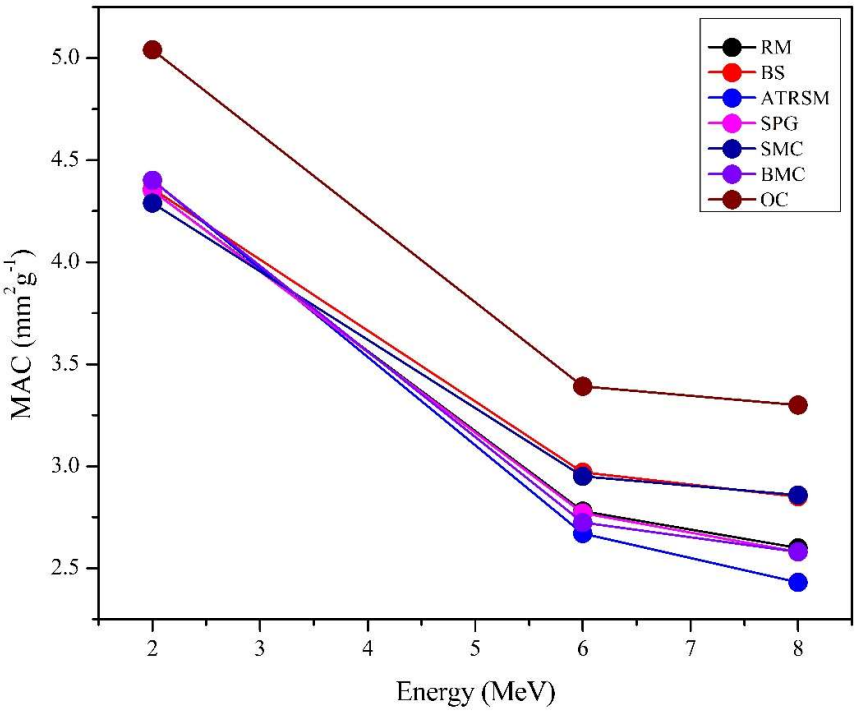
RM
BS
ATRSM
SPG
SMC
BMC
OC
MAC (mm^{2}g^{-1})
Energy (MeV)
5.0
4.5
4.0
3.5
3.0
2.5
2
3
4
5
6
7
8

Fig.11.

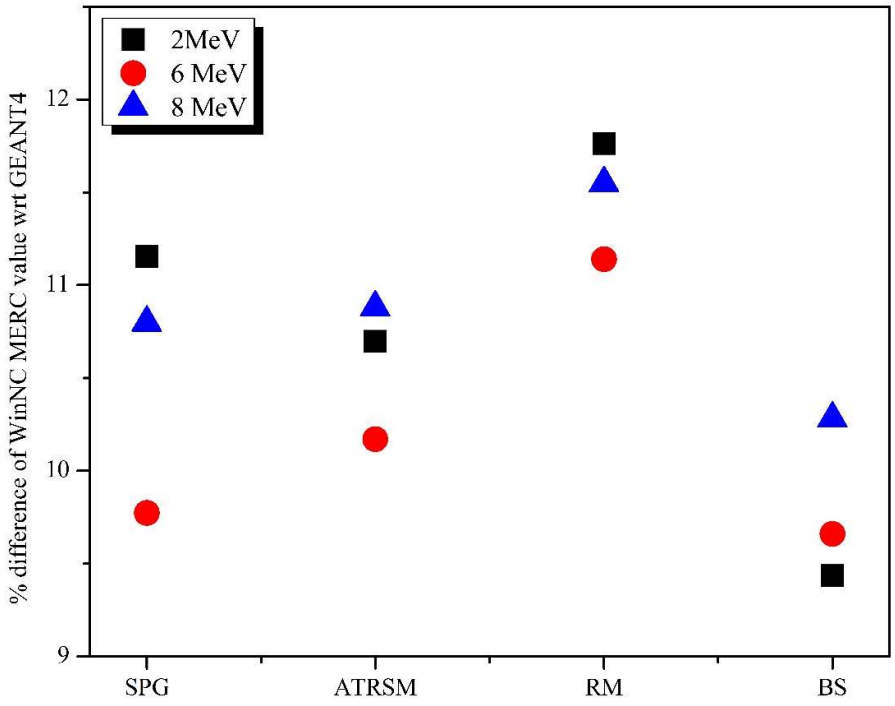
2MeV
6 MeV
8 MeV
% difference of WinNC MERC value wrt GEANT4
12
11
10
9
SPG
ATRSM
RM
BS

Fig.12.

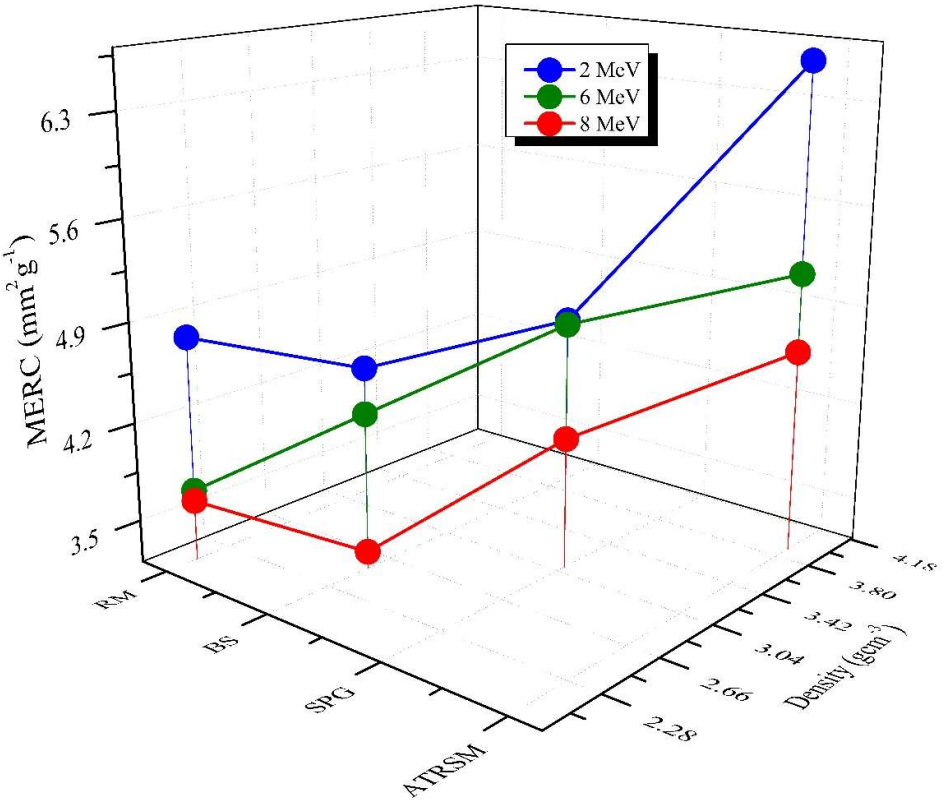
2 MeV
6 MeV
8 MeV
MERC (mm^2 g^{-1})
6.3
5.6
4.9
4.2
3.5
RM
BS
SPG
ATRSM
4.18
3.80
3.42
3.04
2.66
2.28
Density (gcm^{-3})

Fig.13.

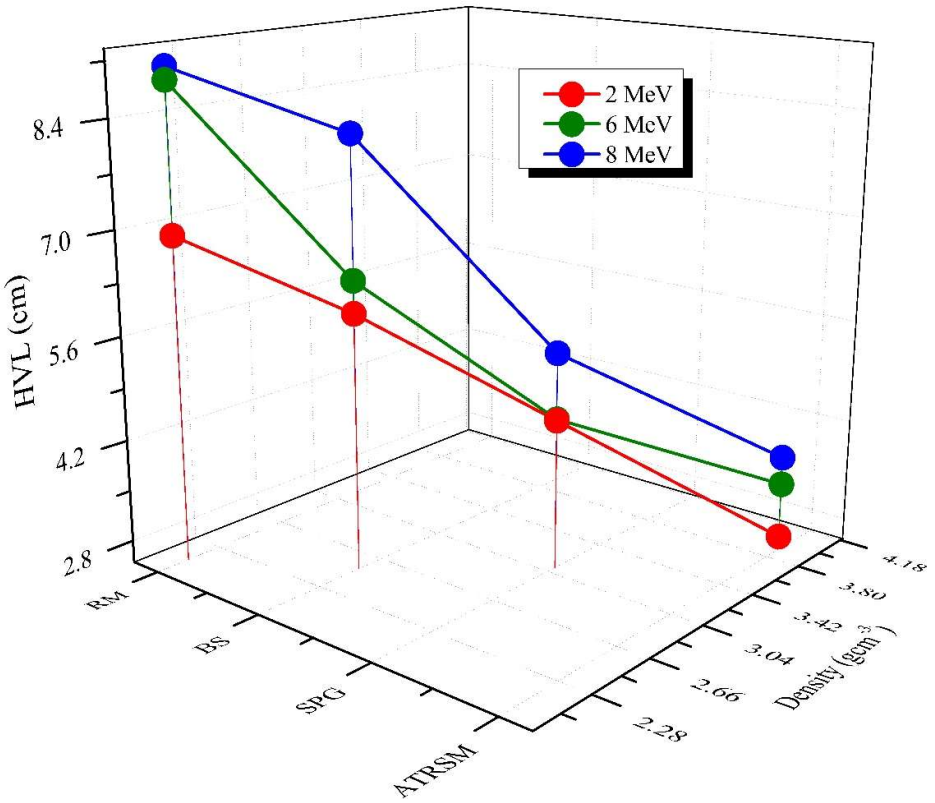
2 MeV
6 MeV
8 MeV
HVL (cm)
8.4
7.0
5.6
4.2
2.8
RM
BS
SPG
ATRSM
4.18
3.80
3.42
3.04
2.66
2.28
Density (gcm^{-3})

Fig.14.

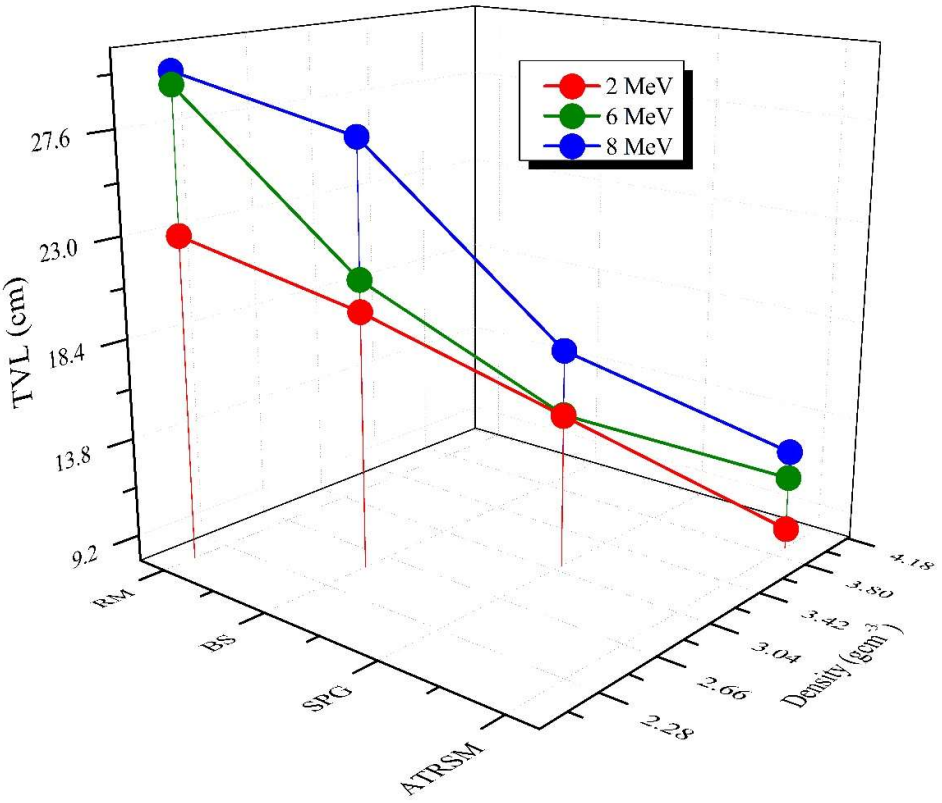

Fig.15.

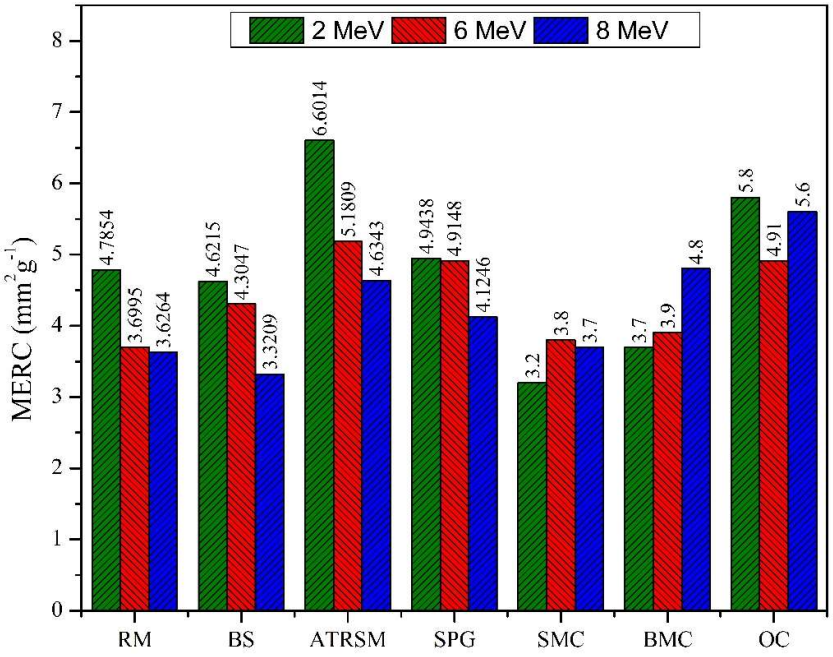

Fig.16